Cellulose-Based Ionogels for Paper Electronics

*Stefan Thiemann, Swetlana J. Sachnov, Fredrik Pettersson, Roger Bollström, Ronald Österbacka, Peter Wasserscheid, and Jana Zaumseil**

A new class of biofriendly ionogels produced by gelation of microcellulose thin films with tailored 1-ethyl-3-methylimidazolium methylphosphonate ionic liquids are demonstrated. The cellulose ionogels show promising properties for application in flexible electronics, such as transparency, flexibility, transferability, and high specific capacitances of 5 to 15 μF cm^{-2}. They can be laminated onto any substrate such as multilayer-coated paper and act as high capacitance dielectrics for inorganic (spray-coated ZnO and colloidal ZnO nanorods) and organic (poly[3-hexylthiophene], P3HT) electrolyte-gated field-effect transistors (FETs), that operate at very low voltages (<2 V). Field-effect mobilities in ionogel-gated spray-coated ZnO FETs reach 75 cm^2 V^{-1} s^{-1} and a typical increase of mobility with decreasing specific capacitance of the ionogel is observed. Solution-processed, colloidal ZnO nanorods and laminated cellulose ionogels enable the fabrication of the first electrolyte-gated, flexible circuits on paper, which operate at bending radii down to 1.1 mm.

1. Introduction

Paper is a cheap, ubiquitous, and biofriendly material that is used as a flexible substrate for many applications in daily life. Modern methods of pulp and paper processing have also substantially reduced the energy consumption associated with paper production.[1] Hence, using paper as a substrate for low-cost, printable, and flexible electronics has been an attractive goal for some time.[2–7] The absorbency and roughness of ordinary paper make it a challenging substrate compared to smooth but more expensive and non-biodegradable plastic sheets, such as polyethylene terephthalate (PET) and polyimide (PI). However, these issues may be overcome by using a recently developed multilayer-coating structure[8] which holds great potential for applications in flexible electronics.[9,10] Furthermore, special micro- and nanocellulose papers, which are transparent and have a much smoother surface than regular paper and a low thermal expansion coefficient, have attracted considerable attention recently as substrates for circuits[11–15] and actuators[16,17] In general, paper is seen as a renewable, biofriendly material whose value and utility is increased substantially by adding extra functionalities such as energy storage and (opto-)electronic circuits.[18]

In order to build electronic circuits on paper, suitable electrode materials, semiconductors and dielectrics are required, which should ideally reproduce the advantageous properties of the paper, e.g., biodegradability, low cost, and flexibility, while maintaining high performance. They should not only be compatible with paper in terms of their mechanical, thermal, and adhesion properties, but should also be processable in the same way. High temperature and vacuum processes are therefore less suitable. One crucial component of an electronic circuit containing many thin-film field-effect transistors (FETs) is the gate dielectric, which determines to a large degree the operating voltage and switching speed. High capacitance dielectrics are ideal for low-voltage FETs.[19] However, most polymeric printable dielectrics (e.g., Cytop, PMMA, PVA) result in relatively low capacitances and are not particularly compatible with paper substrates, while high-permittivity inorganic dielectrics (e.g., Al_2O_3 or HfO_2) require vacuum deposition or sputtering. Here we introduce a new class of cellulose-based ionogels as high capacitance gate dielectrics for electrolyte-gated FETs on paper. These ionogels are produced from microcellulose thin films and tailor-made methylphosphonate ionic liquids, which result in flexible, transferable, and high capacitance dielectrics, that match the advantageous properties of paper while allowing for low-voltage (<2 V) operation of solution-processed inorganic and organic FETs.

Electrolyte-gating has recently emerged as a promising method to obtain low voltage, high performance FETs with solution-processed organic, inorganic, or colloidal semiconductors.[20–26] The traditional gate dielectric of an FET is replaced by an electrolyte that is ionically conducting but electronically insulating. Upon application of a gate voltage, the anions and cations of the electrolyte move toward the gate electrode

S. Thiemann, Prof. J. Zaumseil
Institute of Polymer Materials
Friedrich-Alexander Universität Erlangen-Nürnberg
Martensstraße 7, D-91058, Erlangen, Germany
E-mail: jana.zaumseil@fau.de
S. J. Sachnov, Prof. P. Wasserscheid
Department of Chemical and Bioengineering
Friedrich-Alexander-Universität Erlangen-Nürnberg
Egerlandstraße 3, D-91058, Erlangen, Germany
F. Petterson, Prof. R. Österbacka
Physics, Department of Natural Sciences and Center for Functional Materials
Åbo Akademi University
Porthansgatan 3, 20500, Turku, Finland
R. Bollström
Center for Functional Materials
Laboratory of Paper Coating and Converting
Åbo Akademi University
Porthansgatan 3, 20500, Turku, Finland

DOI: 10.1002/adfm.201302026

and the semiconductor surface, respectively, depending on the polarity of the bias. There they form electric double layers (EDLs). Because the bulk electrolyte remains neutral, the applied gate voltage drops almost entirely over the few-nanometer thick EDLs, leading to very high effective capacitances (several μF cm^{-2}).[27] This allows for the accumulation of large charge carrier densities at low gate voltages and eventually low-voltage operation. Ionic liquids (ILs) are ideal electrolytes for this task due to their high ion concentration and wide electrochemical windows. For the application of electrolyte-gating in integrated circuits on bendable substrates the electrolyte has to be solid yet flexible. This can be achieved by forming electrolyte gels or ionogels, which combine mechanical stability with high ionic conductivity. Out of the large variety of ionogels, recently reviewed by Le Bideau et al.,[28] composites of imidazolium-based ionic liquids (e.g., [EMIM][TFSI], 1-ethyl-3-methylimidazolium bis(trifluoromethylsulfonyl)imide) and small amounts of ABA triblock-copolymers (e.g., poly[styrene-b-methylmethacrylate-b-styrene]) have been employed extensively as printable ionogels for electrolyte-gated FETs on plastic substrates.[20,29–31] Other polymer/IL blends like [EMIM][TFSI] and poly(vinylidene fluoride-*co*-hexafluoropropylene) form free-standing rubbery ionogels that can be cut into shape and laminated onto the intended transistor structure.[32] Importantly, in all cases, the ions of the IL remain mobile within the polymer network and thus the high effective capacitance and fast switching of pure ILs are maintained. Biopolymers, such as cellulose, can also exhibit gelation with certain ionic liquids.[33] Cellulose is the main component of most papers; it is biodegradable and produced from renewable sources at low cost. Thus, obtaining an easy-to-handle ionogel from cellulose, which is compatible with paper as a substrate, is highly advantageous for future paper electronics.

Cellulose dissolves in certain ionic liquids, which are considered non-derivatizing solvents.[33–35] The ability of these ILs to dissolve carbohydrates is mainly attributed to the nucleophilicity of their anions, such as halides, formate, acetate, phosphates and phosphonates,[34,36–42] that are able to disrupt the structure of the biopolymer.[43] In particular, they form a primary solvation shell around the perimeter of the glucose ring.[35] Anions with poor to negligible H-bond acceptor characteristics, such as, e.g., tetrafluoroborate or hexafluorophosphate, are considered non-dissolving. The popular [TFSI]$^-$ ion is also non-dissolving because of its low nucleophilicity and its bulky substituents that impede interactions.[44] Kimizuka et al. described the formation of carbohydrate ionogels from ILs with ether-containing cations.[33] ILs without these ether groups show no gelation. The sugar–cation interaction is weak compared to that of the sugar and anion. It is largely based on the interaction of the weakly acidic hydrogen at the C2 position of the imidazolium ring with the oxygen atoms of the secondary sugar.[35] Moreover, the type of cation modifies the effective nucleophilicity of the IL anion only by the competing interaction of cation–anion vs. biopolymer–anion. Note that low humidity is required for the gelation because water interferes by coordinating to the anions.[45] Overall, carbohydrates such as cellulose can form ionogels with ionic liquids containing suitable anions, however none of these gels have yet been used to form thin, free-standing films or applied as dielectrics in FETs. In the following, we will show how ionogels based on microcellulose and specifically tailored ionic liquids can be produced and applied to form the first low-voltage electrolyte-gated FETs on paper.

2. Results and Discussion

2.1. Fabrication and Properties of Cellulose Ionogels

For the formation of stable cellulose ionogels we used ionic liquids with 1-ethyl-3-methylimidazolium [EMIM] as the cation and a range of methylphosphonates[46] as anions (shown in **Figure 1**a). These anions were specifically chosen for the well-known ability of phosphonates to dissolve or gelate carbohydrates. Methylacetate and ethylene glycol side-chains of different lengths were added to further improve interaction of the IL anions with the cellulose and consequently obtain cellulose/IL ionogels. While ionogels from natural cellulose were easily obtained by mechanically mixing them with the methylphosphonate ILs at 60 °C, we chose microcellulose for this study due to its superior processability (printing/coating) compared to natural cellulose fibres. Microcellulose ionogels were produced by simple drop-casting of pure methylphosphonate or mixed (with [EMIM][TFSI]) ionic liquids onto a thin (80 μm) doctor-bladed microcellulose film on an hexamethyldisilazane (HMDS)-treated glass (see Figure S1, Supporting Information) followed by annealing at 80 °C for 3 h to complete gelation. The final mass ratio of cellulose to ionic liquid was 3:70. The large amount of ionic liquid compared to the cellulose is typical for ionogels and ensures high ionic mobility and high effective capacitance.[20] The obtained ionogels could be cut into any shape and delaminated from the glass slide. They were clear and transparent, and mechanically flexible but robust enough to form freestanding films, as shown in Figure 1b. Due to their soft and slightly sticky surface they could be re-laminated onto any substrate of choice for further characterization or use as a dielectric. Pure [EMIM][TFSI] showed no gelation with microcellulose as expected, while mixtures of [EMIM][TFSI] and [EMIM] methylphosphonate ILs (1:9 by volume) formed ionogels similar to those without [TFSI]. All processing steps were carried out in ambient air and the obtained microcellulose-ionogels could be stored for weeks in air without visible changes or deterioration. For simplicity, we will from now on only mention the anions as characteristic for the ionogels. The cation is always [EMIM].

In order to use these ionogels as high capacitance electrolytes in FETs we first evaluated their electrochemical properties. The electrochemical window in dry air only ranges from –1 V to 1.5 V (see **Figure 2**a), while under inert conditions pure [EMIM] methylphosphonate ILs have a much wider electrochemical window of about 4 V in total. The frequency-dependent impedance characteristics of the ionogels were determined by electrochemical impedance spectroscopy (EIS). Figure 2b shows the phase angle versus frequency (*f*) plots for all cellulose ionogels (Nyquist plots of all ionogels can be found in Figure S2, Supporting Information). They show an almost constant phase angle (–75° to –80°) at frequencies up to 1 kHz that drops to 0°

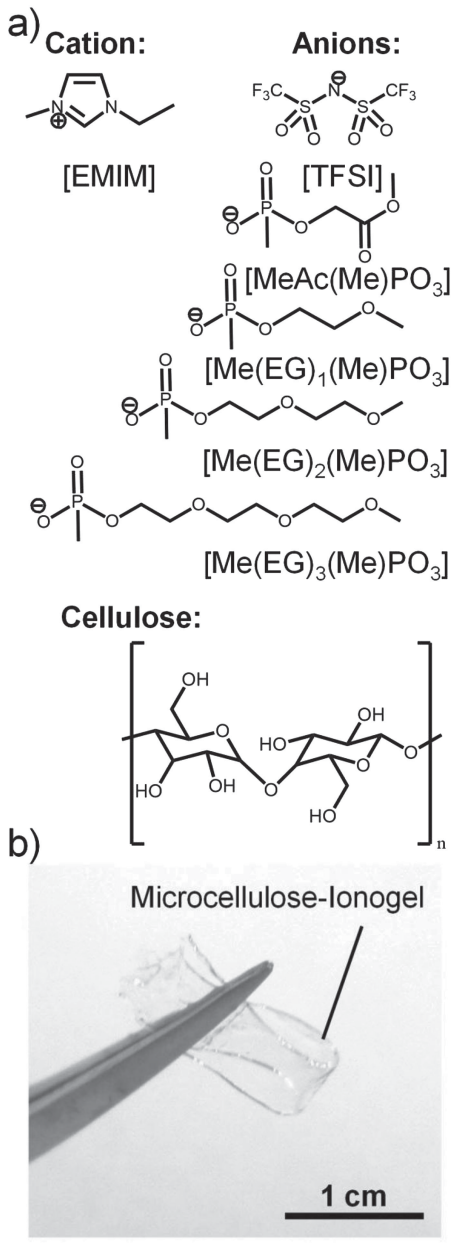

Figure 1. a) Chemical structures of the ionic liquids used for the preparation of microcellulose ionogels and the repeat unit of cellulose. b) Optical image of a free-standing ionogel based on microcellulose and [EMIM][$Me(EG)_2(Me)PO_3$].

at 1 MHz. Small phase angles at high frequencies are indicative of resistor-like behaviour and phase angles close to –90° of capacitive behaviour, which is typical for electrolyte systems.[47] Note that perfect dielectrics should show purely capacitive behaviour, i.e. a phase angle of –90° at low frequencies. For modelling the impedance behaviour of an ionogel a constant phase element has to be included in the equivalent circuit to account for the deviation.[48] Due to the non-negligible conductivity of the ionic liquid and the necessary movement of ions, ideal capacitor behaviour cannot be obtained with ionogels, and

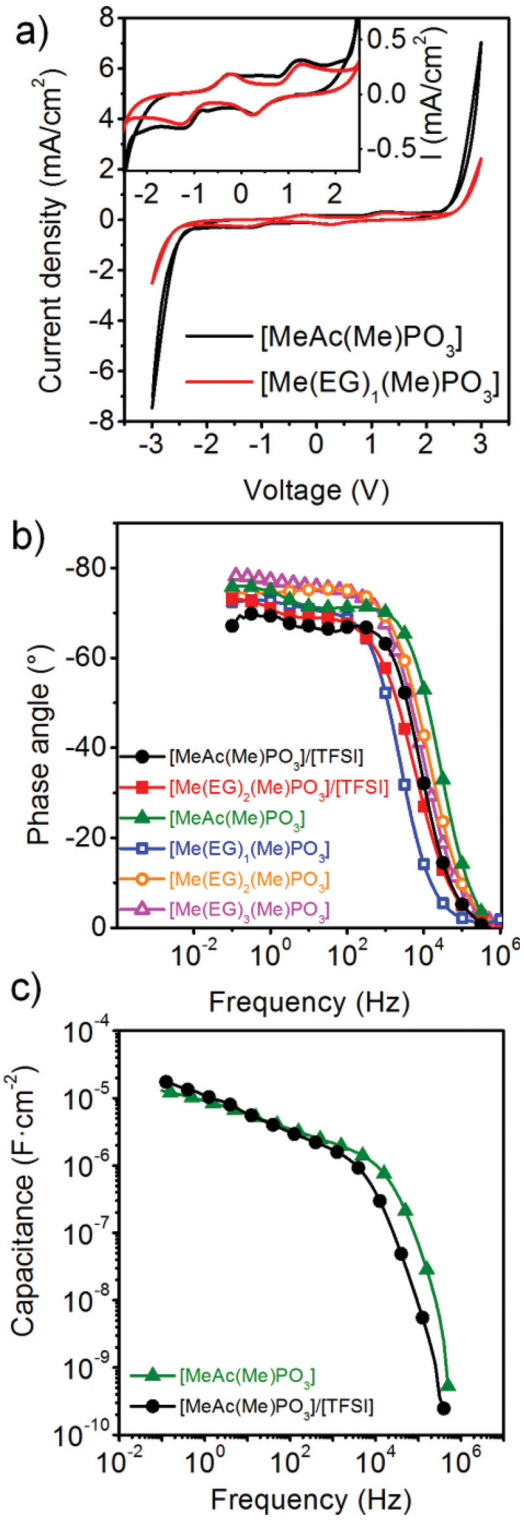

Figure 2. a) Cyclic voltammogram (CV) of cellulose ionogels in dry air with [$MeAc(Me)PO_3$] and [$Me(EG)_2(Me)PO_3$] as anions, sandwiched between to platinum electrodes with a distance of 80 µm; inset shows a zoom-in of the CV for both ionogels from –2.5 V to 2.5 V b) Phase vs frequency plots for all ionogels. c) Extracted frequency-dependent capacitance for [EMIM][$Me(Ac)MePO_3$]/[EMIM][TFSI] and [EMIM][$Me(Ac)MePO_3$] cellulose ionogels.

relatively high leakage currents as well as power dissipation are unavoidable. Due to the formation of EDLs at the interfaces, the specific capacitance of ionogels depends on the applied frequency and bias but not on the film thickness.[49,50] We calculated the frequency-dependent capacitance according to Dasgupta et al.[48] using Equation 1 based on an equivalent circuit consisting of a parallel R–C element connected in series with a resistor and a constant phase element (CPE),

$$C = \frac{-Z''}{|Z|^2 \cdot 2\pi f A} \quad (1)$$

where Z is the impedance, Z'' is the imaginary part of the impedance, f is the frequency and A the electrode area. Figure 2c shows the extracted capacitance versus frequency plots for two ionogels. High capacitances in the μF cm^{-2} range are obtained for frequencies up to 10 kHz. This indicates that the ions within the gel are still highly mobile and can form electric double layers quickly, which is important for the switching speed of FETs gated via ionogels.[51] The specific capacitances of all microcellulose ionogels at the lowest frequency (0.1 Hz) are listed in **Table 1**. The capacitance of the cellulose gel decreases with increasing number of ethylene glycol units and thus increasingly bulky anions, as expected. The mixed IL ionogels show the highest capacitances due to the presence of the small and very mobile [TFSI] anions, which do not interact with the cellulose network.

2.2. Ionogel-Gated Field-Effect Transistors

In order to test whether these new cellulose ionogels can act as high capacitance gate dielectrics, we fabricated FETs with 30 nm spray-coated ZnO as the semiconducting layer and evaporated aluminium electrodes on a rigid substrate (silicon wafer with 300 nm SiO_2). A thin gold sheet served as the gate electrode (**Figure 3**a). The transfer and output characteristics of these FETs measured in dry nitrogen atmosphere are shown in Figure 3b and c for ZnO–FETs with [EMIM][$Me(EG)_1(Me)PO_3$] and mixed [EMIM][$Me(EG)_2(Me)PO_3$]/[EMIM] [TFSI] ionogels as electrolytes. All FETs operate at very low gate voltages between –1.0 V and 1.0 V with small current hysteresis and on/off ratios of 10^4. The maximum on currents for FETs with a W/L = 50 are higher than 1 mA, whereas the gate leakage currents are within a range of 10^{-7}–10^{-8} A, which is typical for electrolyte-gated FETs with an un-patterned semiconductor. The off currents and leakage currents can be reduced and thus the on/off ratios improved by careful patterning of the semiconductor and the dielectric (e.g., by printing) to minimize unnecessary overlap with the gate electrode. The observed current hysteresis is a result of the slow ionic movement and decreases with decreasing sweep rate. Complete transfer and output characteristics of all ionogel-gated ZnO–FETs are shown in Figures S3–S8 of the Supporting Information. Turn-on and threshold voltages (see Table 1) are negative, confirming the expected n-doping of the ZnO thin film.[52] All FETs exhibit standard output characteristics with linear current increase at small source–drain voltages (V_{DS} < 0.2 V) and current saturation at high source–drain voltages. Linear field-effect mobilities were calculated according to

$$\mu_{lin} = \frac{dI_{DS}}{dV_G} \cdot \frac{L}{WC_i V_{DS}} \quad (2)$$

and saturation field-effect mobilities using

$$\mu_{sat} = \frac{dI_{DS}}{dV_G} \cdot \frac{L}{WC_i} \cdot \frac{1}{(V_G - V_{TH})} \quad (3)$$

with W – channel width, L – channel length, C_i – specific capacitance of the ionogel, V_G – gate voltage, V_{TH} – threshold voltage, V_{DS} – source–drain voltage.

For calculation of the field-effect mobilities, the specific capacitance C_i of the ionogel is required. Since the formation of the EDL and therefore the effective capacitance of the ionogel depends on the applied voltage and the nature of the interface, this value should be determined in the actual device rather than using a quasi-static value from EIS obtained at zero bias and with two platinum electrodes. Xie et al. developed a method by which the displacement current (i.e., the gate current) at high sweep rates is used to estimate the number of injected charges and consequently the capacitance.[53] For this, source and drain electrode are grounded and the displacement current (I_{disp}) versus gate voltage is measured at different sweep rates (dV_G/dt) (see Figure S9, Supporting Information). Using Equation 4, the gate voltage dependent capacitances can be determined:[27,53,54]

Table 1. Cellulose ionogel capacitances (Cap), On-voltages (V_{ON}), threshold voltages (V_{Th}), linear (μ_{lin}), and saturation mobilities (μ_{sat}) including respective standard deviations (dev) for spray-coated ZnO-FETs gated via various ionogels, represented by their anions; the cation is always [EMIM].

	Cap [μF cm^{-2}][a)]	Cap [μF cm^{-2}][b)]	V_{ON} [V]	dev	V_{TH} [V]	dev	μ_{lin} [cm^2 V^{-1} s^{-1}]	dev	μ_{sat} [cm^2 V^{-1} s^{-1}]	dev
[$MeAc(Me)PO_3$]/[TFSI]	15.6	18.4	–0.57	0.13	–0.03	0.18	8.9	1.6	7.7	0.6
[$Me(EG)_2(Me)PO_3$]/[TFSI]	11.7	16.5	–0.68	0.06	–0.17	0.07	12.5	1.7	11.2	1.7
[$MeAc(Me)PO_3$]	11.2	13.0	–0.64	0.19	–0.13	0.09	20.4	8.1	21.2	7.8
[$Me(EG)_1(Me)PO_3$]	6.8	8.9	–0.68	0.23	–0.17	0.12	27.3	3.6	25.9	8.2
[$Me(EG)_2(Me)PO_3$]	6.5	8.6	–0.66	0.12	–0.18	0.08	33.9	8.9	33.1	10.6
[$Me(EG)_3(Me)PO_3$]	4.6	8.5	–0.85	0.21	–0.25	0.10	60.5	8.9	75.2	6.9

[a)]Capacitances extracted from displacement current measurements (V_G = 1 V) according to Xie et al;[53] [b)]Capacitances determined by impedance spectroscopy according to Dasgupta et al.[48]

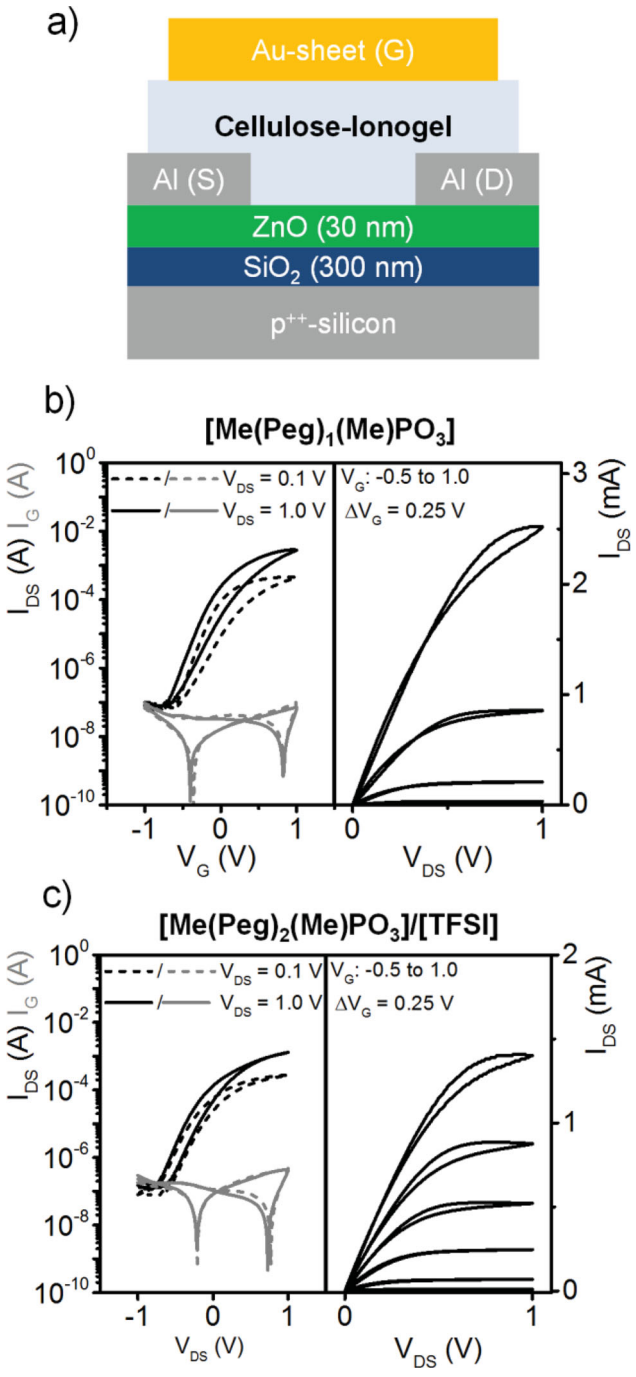

Figure 3. a) Schematic illustration of cellulose ionogel-gated zinc oxide thin film FET (S – source electrode, D – drain electrode, G – gate electrode). Transfer curves (left) for linear (V_{DS} = 0.1 V, dashed line) and saturation (V_{DS} = 1.0 V, solid line) regime and output curves (right) of spray-coated ZnO–FETs with (a) [EMIM][Me(EG)$_1$(Me)PO$_3$] and b) mixed [EMIM] [Me(EG)$_2$(Me)PO$_3$]/[EMIM][TFSI] cellulose ionogels (gate voltage sweep rate 80 mV s^{-1}).

$$I_{disp}(V_G) = A \cdot C_i(V_G) \frac{dV_G}{dt} \quad (4)$$

The extracted specific capacitances of the cellulose ionogels at V_G = 1 V vary from 15.6 µF cm^{-2} for cellulose ionogels with mixed ionic liquids, that is, [EMIM][MeAc(Me)PO$_3$]/[EMIM][TFSI], to 4.6 µF cm^{-2} for ionogels with [EMIM][Me(EG)$_3$(Me)PO$_3$] (see Table 1). Note that the capacitances increase with gate voltage for all ionogels, which could be due to improved packing of the ions at the IL/semiconductor interface at higher gate fields. The capacitance values obtained from the displacement current method are slightly lower than those obtained from EIS measurements but show the same overall trends. We used the former gate voltage-dependent capacitance to calculate the electron field-effect mobilities listed in Table 1 and evaluate the influence of capacitance on the turn-on behaviour of the FETs. Both on-voltages and threshold voltages decreased linearly with $1/C_i$ as expected (see **Figure 4**a). In agreement with previous results with other pure ILs[55] the electron field-effect mobility in ionogel-gated ZnO–FETs decreased with increasing ionogel capacitance (see Figure 4b and Figure S10, Supporting Information) from 75 to 8 cm^2 V^{-1} s^{-1}. Note that this effect cannot result from any error in the capacitance calculation; the maximum transconductance dI_{DS}/dV_G of the ZnO–FETs itself decreases with increasing ionogel capacitance (see Figure S11, Supporting Information). For device applications, the final channel

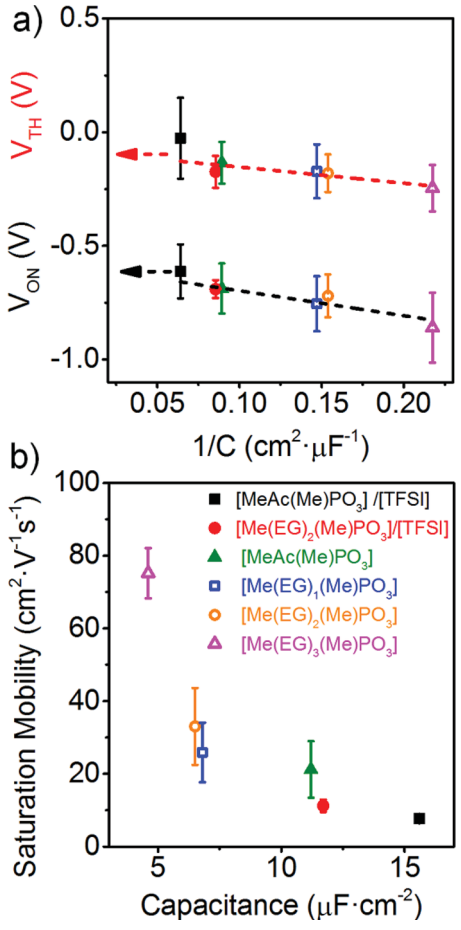

Figure 4. a) Threshold voltage and on-voltage vs. inverse of the specific capacitance for ZnO–FETs with different ionogels (indicated by their anions) including linear fits (red and black dashed lines). b) Saturation electron field-effect mobility vs. the specific capacitance for all ionogel-gated ZnO–FETs.

resistance and switching speed are most important. In order to maximize those, higher capacitance ionogels such as the mixed IL ionogels are ultimately preferable.

Ionogel-gated ZnO–FETs are stable in nitrogen atmosphere over time and can be switched frequently with stable on/off ratios (Figure S12 and S13, Supporting Information) while the threshold voltages shift to more positive values. This effect was also observed for ZnO–FETs gated via pure ionic liquids that contained imidazolium cations with an acidic H atom at the C2 position[55] and does not result from the presence of the cellulose. Similar to our previous results, the transistor performance decreases rapidly in air, when water is absorbed by the ionogel. The protic environment leads to surface reactions with the ZnO as also observed by Yuan et al.[56] However, this degradation can be easily avoided by passivating the ZnO surface, e.g., with HMDS (see Figure S14, Supporting Information).

The application of these new cellulose-based ionogels in FETs is not limited to inorganic or n-type semiconductors. **Figure 5**a illustrates an ionogel-gated FET with spincoated rr-P3HT (regio-regular poly[3-hexylthiophene]) as a p-type polymer semiconductor on pre-patterned gold electrodes. A laminated cellulose ionogel with mixed ionic liquid [EMIM][MeAc(Me)PO_3]/[EMIM][TFSI] as the electrolyte and a gold sheet as the gate electrode complete the device. The transfer and output characteristics of such an FET are shown in Figure 5b,c. They are similar to those of P3HT–FETs gated via synthetic ionogels.[31,32] Although the methylphosphonate anions coordinate to the cellulose within the ionogel unlike the cations, there are clearly enough free anions—in particular the [TFSI] anions—to electrochemically dope the P3HT film and turn the transistor on and off, proving the general applicability of cellulose ionogels for electrolyte-gated FETs.

2.3. Flexible Ionogel-Gated FETs on Paper

The microcellulose ionogels are soft and conformable, which makes them ideal to fabricate flexible transistors on paper. To demonstrate this, we used a recently developed multilayer-coated paper as a flexible substrate.[8] As a low-temperature alternative to the high-temperature spray-pyrolysis of ZnO we chose colloidal ZnO nanorods as the semiconductor, which can be synthesized via a sol–gel route and deposited from solution at low temperatures.[57] Previously we showed that ZnO nanorod layers can reach high electron mobilities when aligned and electrolyte-gated with ionic liquids.[58] Due to the residual roughness of the uncalendered multilayer-coated paper (≈450 nm), the film morphology of the dropcast ZnO nanorods is very non-uniform (see **Figure 6**a). The laminated cellulose ionogel could nevertheless conform to this very coarse surface and electrolyte-gating mitigated the detrimental effects of surface roughness to some degree because the EDL is always formed directly at the nanorod/ionogel interface. In order to fabricate complete ZnO nanorod FETs on paper we used evaporated gold electrodes and a side-gate geometry (shown in Figure 6a,b). Here the gate is not on top of the channel but located next to the FET on the substrate. This means that the ions have to move further to create EDLs, which reduces the switching speed. Hence using a side-gate geometry without a large sweep rate-dependent hysteresis is only possible when the ionic mobility within the ionogel is high. To achieve this we used the mixed ionic liquid gels containing [$Me(EG)_2(Me)PO_3$] and [TFSI] anions. Nevertheless, side-gated FETs respond more slowly than those with a top gate.

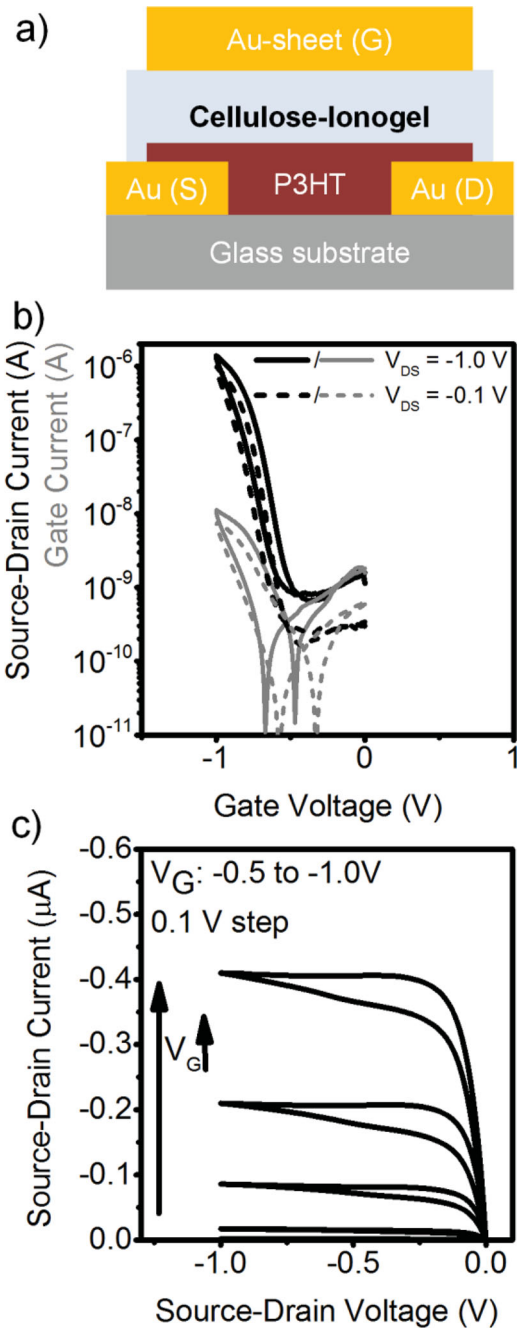

Figure 5. a) Schematic structure of ionogel-gated P3HT–FET (S – source electrode, D – drain electrode, G – gate electrode). b) Transfer and c) output characteristics with [EMIM] [$Me(EG)_2(Me)PO_3$]/[EMIM][TFSI] cellulose-ionogel (W/L = 1000, sweep rate: 25 mV s^{-1}).

The ZnO nanorod FETs turn on at 0.8 V and on/off ratios of about 10^2 are obtained (Figure 6d). The electron mobility is relatively low (μ_{lin} = 0.03 cm^2 V^{-1} s^{-1}) due to the short (length

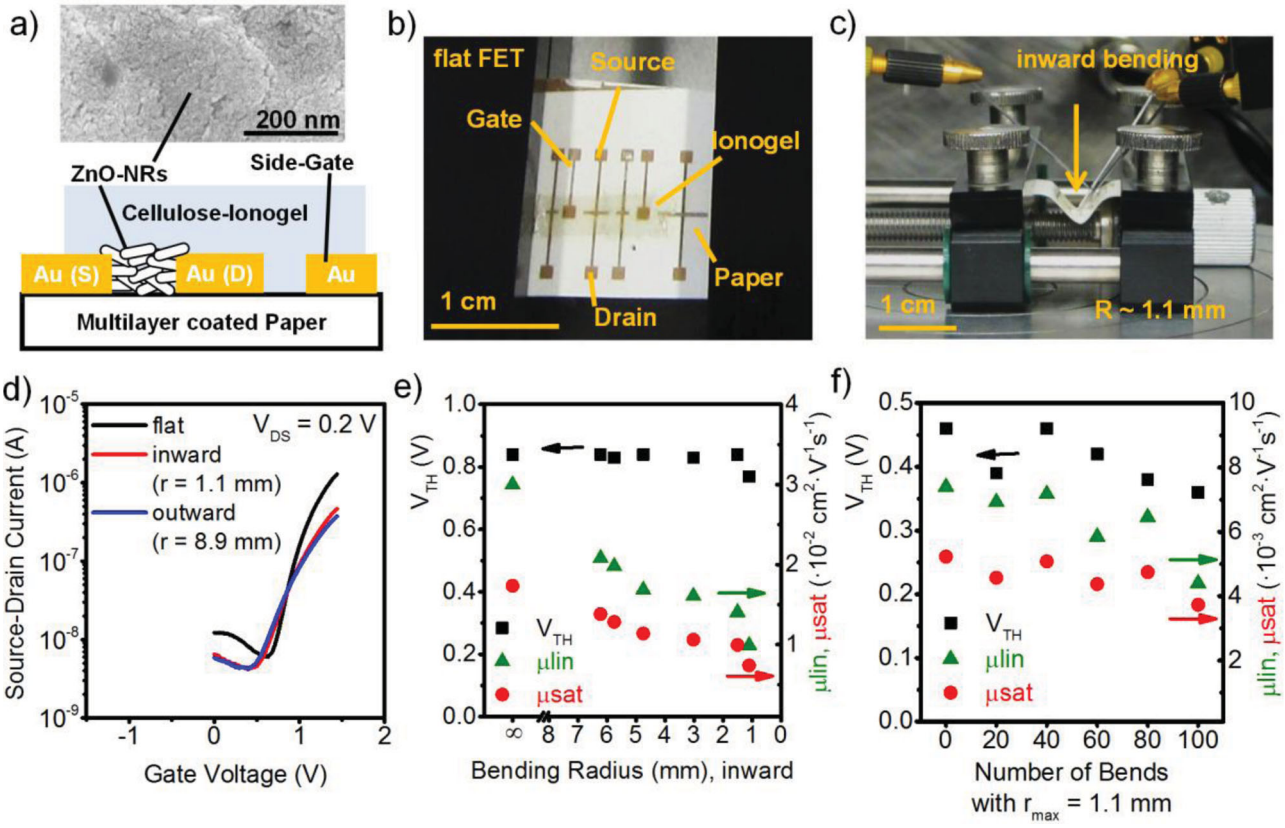

Figure 6. a) Schematic illustration of electrolyte-gated FET with ZnO nanorods and side gate on multilayer-coated paper with laminated cellulose ionogel; inset: SEM image of short ZnO nanorods (length 14 nm) on paper. b) Optical image of ZnO nanorod FET on multilayer-coated paper with laminated ionogel before bending and c) during inward bending with a bending radius of 1.1 mm. d) Transfer characteristics before and during inward (radius 1.1 mm) and outward bending (radius 8.9 mm) at V_{DS} = 0.2 V (sweep rate 45 mV s^{-1}). Threshold voltages (V_{TH}) and linear and saturation electron field-effect mobilities vs bending radius (e) and vs number of bends (bending from flat to bending radius of 1.1 mm) (f) for ionogel-gated ZnO nanorod FET on multilayer-coated paper substrate with [EMIM] [$Me(EG)_2(Me)PO_3$]/[EMIM][TFSI] ionogel in nitrogen atmosphere.

14 nm) and very disordered nanorods. Under bending stress (see Figure 6c) the performance of the FETs degrades somewhat. For inward bending, that is, compressive strain, the linear field-effect mobility drops with decreasing bending radius r down to 0.01 cm^2 V^{-1} s^{-1} at r = 1.1 mm, shown in Figure 6e. The transistors continue to operate after 100 bends but the linear mobility decreases by almost an order of magnitude and the threshold voltage shifts slightly (see Figure 6f). When bending is performed in the opposite direction, crack formation in the nanorod thin film and thus device failure occur almost immediately. The smallest outward bending radius for an operating FET was 8.5 mm with a linear mobility of μ_{lin} = 0.007 cm^2 V^1 s^{-1}. Although cracks are created in the ZnO nanorod layer, the transistors resume to operate after returning to the initial position albeit with reduced electron mobilities. Note, that we do not observe any changes or damage to the ionogel layer after bending and the performance loss can be attributed solely to the cracking of the ZnO nanorod layer.

The performance of flexible ZnO nanorod transistors on paper can be further improved by using longer nanorods (87 nm) and calendered, extra smooth paper substrates (roughness 57 nm) as shown in Figures S15 and S16 (Supporting Information). The linear electron mobilities in these devices reach 0.15 cm^2 V^1 s^{-1} and inward and outward bending radii of down to 1.2 mm and 3.9 mm, respectively, are achievable.

In order to further evaluate the feasibility of ionogel-based circuits on paper, we built a simple resistor-loaded inverter with a ZnO nanorod FET on paper with [EMIM][MeAc(Me)PO_3]/[EMIM][TFSI]/cellulose ionogel in side-gate geometry. The transistor is connected in series with a resistor of 4.72 MΩ. Typical inverter characteristics are observed with a relatively large hysteresis, possibly due to the side-gate geometry and thus longer response time (**Figure 7**a). The output voltage switches from 0.2 V to 1.2 V with a gain of 2. The response of the inverter to a sine wave input voltage is shown in Figure 7b (V_{DD} = 1.3 V, frequency f = 0.3 Hz). For this side-gate FET the low mobility of the ZnO nanorod layer (short nanorods) and the large channel length of 40 μm limit the inverter performance rather than the ionogel.

3. Conclusions

We have introduced a new class of ionogels based on microcellulose and various methylphosphonate ionic liquids that are easy to process and show promising properties for application in flexible electronics, such as transparency, flexibility,

transferability, and high capacitance. We have demonstrated their performance as high capacitance dielectrics in low voltage inorganic and organic FETs and simple circuits, including flexible FETs on paper. Ionogels based on anion mixtures of [TFSI] and methylphosphonates are well-suited for side-gated FETs due to their higher ionic mobility, while ionogels with lower specific capacitances result in higher electron mobilities in spray-coated ZnO FETs. Cellulose-based ionogels match the performance of more commonly used ionogels based on synthetic copolymers in terms of specific capacitance and response time, while being biofriendly and derived from cheap and renewable resources. Apart from FET dielectrics they may also find application in paper-based supercapacitors or actuators.

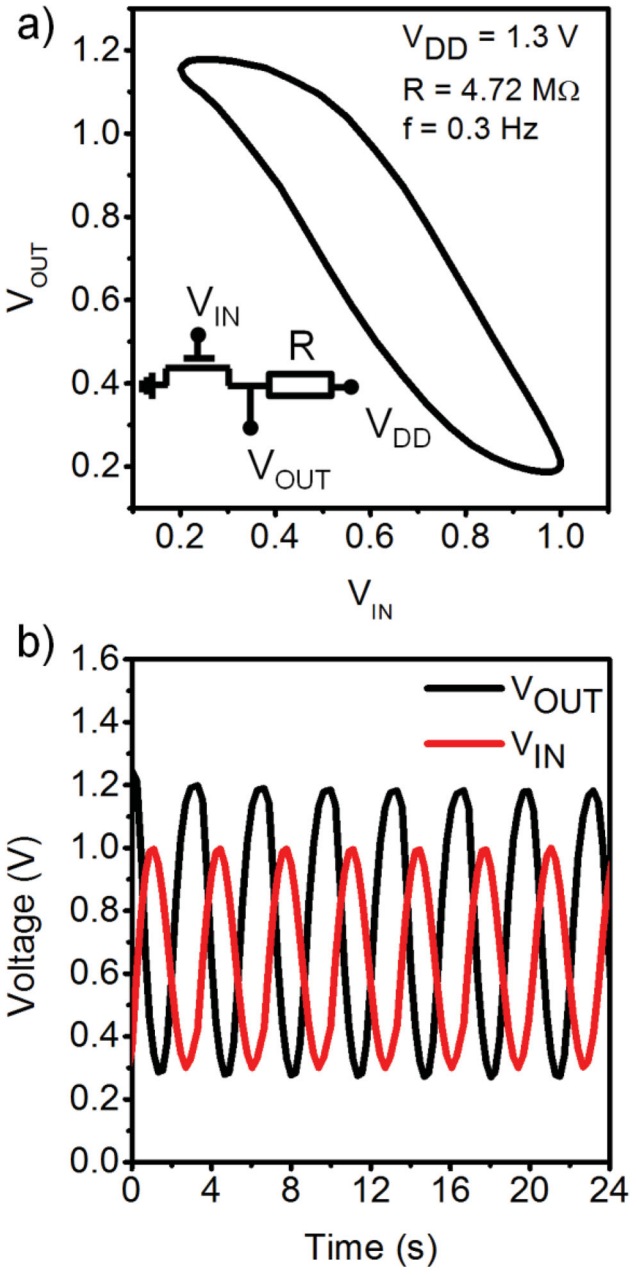

Figure 7. a) Transfer curve of a resistor-loaded inverter with an ionogel-gated ZnO nanorod FET on paper with a gain of 2 at V_{DD} = 1.3 V. Inset: schematic inverter circuit. b) V_{IN} and V_{OUT} vs. time at V_{DD} = 1.3 V with sine wave voltage input of 0.3 Hz.

4. Experimental Section

Preparation of Cellulose Ionogels: [EMIM][TFSI] (1-ethyl-3-methylimidazolium bis(trifluoromethylsulfonyl)imide) was purchased from Merck KGaA (high purity grade). Methylphosphonate ionic liquids (ILs) with [EMIM] as the cation were synthesized from functionalized methyl methylphosphonate esters by demethylation reaction as described by Sachnov et al.[46] List of IUPAC names of the IL anions followed by their abbreviation: (2-methoxy-2-oxoethyl methylphosphonate) [MeAc(Me)PO_3], 2-methoxyethyl methylphosphonate [Me(EG)$_1$(Me)PO_3], 2-(2-methoxy-ethoxy)ethyl methylphosphonate [Me(EG)$_2$(Me)PO_3], 2-(2-(2-methoxyethoxy)ethoxy)ethyl methylphosphonate [Me(EG)$_3$(Me)PO_3].

Microscope glass slides (2.5 cm × 2.6 cm) were treated with HMDS (hexamethyldisilazane) (water contact angle = 75°) in order to decrease the adhesion of the ionogel to the glass and allow for peel-off. An aqueous microcellulose dispersion (Arbocel MF 40–7, J. Rettenmaier & Söhne GmbH + Co KG) was doctor-bladed onto the glass slides and heated at 80 °C for 5 min resulting in a thin white film of the microcellulose with 12 g m^{-2} (see Figure S1, Supporting Information). The microcellulose fibers have an average length of about 8 µm and a low aspect ratio. Methylphosphonate ILs or mixed ILs ([EMIM][MeAc(Me)PO_3]:[EMIM][TFSI] = 9:1 and [EMIM][Me(EG)$_n$(Me)PO_3]:[EMIM][TFSI] = 9:1) were slowly dropped onto the dried microcellulose film. Homogeneous infiltration of the IL was completed after a few minutes. Subsequently the films were annealed for 3 h at 80 °C to induce gelation. The obtained ionogel film (thickness 80 µm) was cut into stripes, delaminated and transferred onto platinum electrodes for impedance spectroscopy or onto a semiconductor layer for FET fabrication. All processing steps were carried out in ambient air.

ZnO Thin Films and ZnO Nanorods: ZnO thin films (thickness ≈ 30 nm) were fabricated by spray-coating a methanolic zincacetate solution onto Si/SiO_2 (300 nm) wafers at 400 °C in air as described in detail elsewhere.[55] ZnO nanorods were synthesized following a modified recipe by Voigt et al.[59] Briefly, zincacetate dihydrate (3.29 g, Sigma Aldrich) and potassium hydroxide (1.35 g, Sigma Aldrich) were dissolved separately in 30 ml of methanol at 60 °C. The two solutions were mixed and refluxed at 60 °C for 24 h. After stopping the reaction by adding excess methanol the obtained nanorod dispersion was stored at 8 °C for 12 h. Short ZnO nanorods (length 14 nm, diameter 5 nm) were washed three times with methanol to remove byproducts. Longer ZnO nanorods (length 87 nm, diameter 9.2 nm) were synthesized according to Sun et al.[57] Zincacetate dihydrate (4.35 g) and potassium hydroxide (1.78 g) were dissolved separately in 40 mL of methanol at 60 °C. The two solutions were mixed and stirred for 2 h before the solvent volume was reduced to a tenth. This concentrated solution was stirred at 60 °C for 24 h before further growth was stopped and the obtained nanorods were washed as described above. For both types of ZnO nanorods the final precipitate after centrifugation was dispersed in a chloroform:methanol (3:1) solution at a concentration of 70 mg/mL. Adding butylamine (1 µL per 1 mg ZnO) followed by bath sonication for 10 min gave stable and homogeneous dispersions.

Device Fabrication and Characterization: Spray-coated ZnO–FET on silicon substrates were completed by deposition of 50 nm of aluminium on top of the ZnO thin film by e-beam evaporation through a polyimide shadow mask to pattern source and drain electrodes (channel length L = 30 µm, channel width W = 1500 µm, W/L = 50). Bottom contact source–drain and side gate electrodes (50 nm of Au evaporated through a polyimide shadow mask with W/L = 50 and channel length of 20 and 40 µm) were used for FETs on calendered and uncalendered multilayer-coated paper (mean roughness 57 nm and 450 nm, respectively). Calendering of the paper was carried out with a laboratory scale soft nip calender, applying three passes in a

soft nip at a line load of 120 kN m^{-1} and at a temperature of 70 °C. ZnO nanorods were deposited by drop-casting of the dispersion onto the channel area followed by annealing in air at 150 °C for 30 min to remove butylamine. Regio-regular P3HT (Plextronics, M_w = 54 000–75 000 g/mol) was spincoated from dichlorobenzene (3 mg/mL) on a glass substrate with photolithographically defined gold source/drain electrodes (L = 20 µm, W = 20 mm) in nitrogen atmosphere.

Ionogels were laminated onto the devices (ZnO and P3HT) and either a thin gold-sheet was used as a top gate (spray-coated ZnO FETs and P3HT FETs) or a gold side-gate was employed (ZnO nanorod FETs on paper). Current-voltage characteristics of ionogel-gated ZnO–FETs were measured with an Agilent 4155C parameter analyzer or with an Agilent 41421B DC source/monitor analyzer. Resistor-loaded inverters were realized with an external resistor (4.72 MΩ). Unless otherwise noted, all samples were stored and all measurements were carried out in a dry nitrogen glovebox.

Impedance measurements and cyclic voltammetry (CV) of ionogels were performed with a Gamry Instruments Reference 600 potentiostat/galvanostat/ZRA in dry air. For that the ionogels were sandwiched between conventional platinum electrodes (4 mm diameter). The sweep rate for all CV-measurements was 100 mV s^{-1}. Impedance spectra were recorded for frequencies between 1 MHz and 0.1 Hz with an oscillation amplitude of 10 mV and dc-bias of 0 V. Scanning electron images of the ZnO nanorods on paper were obtained with a field emission scanning electron microscope (Hitachi FE-SEM S4800).

Supporting Information

Supporting Information is available from the Wiley Online Library or from the author.

Acknowledgements

This research was funded by the Deutsche Forschungsgemeinschaft (DFG) via the Research Training Group 'Disperse Systems for Electronic Applications' (GRK 1161) and the Cluster of Excellence 'Engineering of Advanced Materials' (EXC 315). Further financial support was provided by the Academy of Finland through the Center of Excellence program (#141115). The authors are grateful to H. Hildebrand for help with scanning electron microscopy and to Evonik Industries AG. Imerys Minerals Ltd., UK, Paramelt B. V., NL, StoraEnso, FI, and BASF, GER are acknowledged for providing the materials for multilayer-coated paper. Tekes funding (Grant 40092/09) is acknowledged for the pilot scale coatings of multilayer-coated paper.

Received: June 13, 2013
Revised: July 22, 2013
Published online: September 18, 2013

[1] D. Gavrileseu, *Environ. Eng. Manag. J.* **2008**, *7*, 537.
[2] D. Tobjörk, R. Österbacka, *Adv. Mater.* **2011**, *23*, 1935.
[3] F. Eder, H. Klauk, M. Halik, U. Zschieschang, G. Schmid, C. Dehm, *Appl. Phys. Lett.* **2004**, *84*, 2673.
[4] E. Fortunato, N. Correia, P. Barquinha, L. Pereira, G. Goncalves, R. Martins, *IEEE Electron Device Lett.* **2008**, *29*, 988.
[5] U. Zschieschang, T. Yamamoto, K. Takimiya, H. Kuwabara, M. Ikeda, T. Sekitani, T. Someya, H. Klauk, *Adv. Mater.* **2011**, *23*, 654.
[6] R. F. P. Martins, A. Ahnood, N. Correia, L. M. N. P. Pereira, R. Barros, P. M. C. B. Barquinha, R. Costa, I. M. M. Ferreira, A. Nathan, E. E. M. C. Fortunato, *Adv. Funct. Mater.* **2013**, *23*, 2153.
[7] J. P. Rolland, D. A. Mourey, *MRS Bull.* **2013**, *38*, 299.
[8] R. Bollström, A. Määttänen, D. Tobjörk, P. Ihalainen, N. Kaihovirta, R. Österbacka, J. Peltonen, M. Toivakka, *Org. Electron.* **2009**, *10*, 1020.
[9] D. Tobjörk, H. Aarnio, P. Pulkkinen, R. Bollström, A. Määttänen, P. Ihalainen, T. Mäkelä, J. Peltonen, M. Toivakka, H. Tenhu, R. Österbacka, *Thin Solid Films* **2012**, *520*, 2949.
[10] P. Ihalainen, A. Määttänen, J. Järnström, D. Tobjörk, R. Österbacka, J. Peltonen, *Ind. Eng. Chem. Res.* **2012**, *51*, 6025.
[11] J. Huang, H. Zhu, Y. Chen, C. Preston, K. Rohrbach, J. Cumings, L. Hu, *ACS Nano* **2013**, *7*, 2106.
[12] H. Zhu, Z. Xiao, D. Liu, Y. Li, N. J. Weadock, Z. Fang, J. Huang, L. Hu, *Energ. Environ. Sci.* **2013**, *6*, 2105.
[13] Y. J. Kang, S.-J. Chun, S.-S. Lee, B.-Y. Kim, J. H. Kim, H. Chung, S.-Y. Lee, W. Kim, *ACS Nano* **2012**, *6*, 6400.
[14] K. Yu Jin, C. Haegeun, H. Chi-Hwan, K. Woong, *Nanotechnology* **2012**, *23*, 065401.
[15] A. Brandt, S. Pohlmann, A. Varzi, A. Balducci, S. Passerini, *MRS Bull.* **2013**, *38*, 554.
[16] J. Kim, S. Yun, Z. Ounaies, *Macromolecules* **2006**, *39*, 4202.
[17] J. Kim, S. Yun, S. K. Mahadeva, K. Yun, S. Y. Yang, M. Maniruzzaman, *Sensors* **2010**, *10*, 1473.
[18] G. Zheng, Y. Cui, E. Karabulut, L. Wågberg, H. Zhu, L. Hu, *MRS Bull.* **2013**, *38*, 320.
[19] R. P. Ortiz, A. Facchetti, T. J. Marks, *Chem. Rev.* **2010**, *110*, 205.
[20] J. H. Cho, J. Lee, Y. Xia, B. Kim, Y. He, M. J. Renn, T. P. Lodge, C. D. Frisbie, *Nat. Mater.* **2008**, *7*, 900.
[21] T. Fujimoto, K. Awaga, *Phys. Chem. Chem. Phys.* **2013**, *15*, 8983.
[22] J. Pu, Y. Yomogida, K.-K. Liu, L.-J. Li, Y. Iwasa, T. Takenobu, *Nano Lett.* **2012**, *12*, 4013.
[23] B. Nasr, D. Wang, R. Kruk, H. Rösner, H. Hahn, S. Dasgupta, *Adv. Funct. Mater.* **2013**, *23*, 1750.
[24] Y. Yomogida, J. Pu, H. Shimotani, S. Ono, S. Hotta, Y. Iwasa, T. Takenobu, *Adv. Mater.* **2012**, *24*, 4392.
[25] K. Hong, S. H. Kim, K. H. Lee, C. D. Frisbie, *Adv. Mater.* **2013**, *25*, 3413.
[26] M. Ha, Y. Xia, A. A. Green, W. Zhang, M. J. Renn, C. H. Kim, M. C. Hersam, C. D. Frisbie, *ACS Nano* **2010**, *4*, 4388.
[27] S. H. Kim, K. Hong, W. Xie, K. H. Lee, S. Zhang, T. P. Lodge, C. D. Frisbie, *Adv. Mater.* **2012**, *25*, 1822.
[28] J. Le Bideau, L. Viau, A. Vioux, *Chem. Soc. Rev.* **2011**, *40*, 907.
[29] J. H. Cho, J. Lee, Y. He, B. S. Kim, T. P. Lodge, C. D. Frisbie, *Adv. Mater.* **2008**, *20*, 686.
[30] J. Lee, L. G. Kaake, J. H. Cho, X. Y. Zhu, T. P. Lodge, C. D. Frisbie, *J. Phys. Chem. C* **2009**, *113*, 8972.
[31] Y. Xia, W. Zhang, M. Ha, J. H. Cho, M. J. Renn, C. H. Kim, C. D. Frisbie, *Adv. Funct. Mater.* **2010**, *20*, 587.
[32] K. H. Lee, M. S. Kang, S. Zhang, Y. Gu, T. P. Lodge, C. D. Frisbie, *Adv. Mater.* **2012**, *24*, 4457.
[33] N. Kimizuka, T. Nakashima, *Langmuir* **2001**, *17*, 6759.
[34] R. P. Swatloski, S. K. Spear, J. D. Holbrey, R. D. Rogers, *J. Am. Chem. Soc.* **2002**, *124*, 4974.
[35] D. R. MacFarlane, J. M. Pringle, K. M. Johansson, S. A. Forsyth, M. Forsyth, *Chem. Commun.* **2006**, 1905.
[36] M. Abe, Y. Fukaya, H. Ohno, *Green Chem.* **2010**, *12*, 1274.
[37] D. Zhao, H. Li, J. Zhang, L. Fu, M. Liu, J. Fu, P. Ren, *Carbhyd. Polym.* **2012**, *87*, 1490.
[38] H. Zhang, J. Wu, J. Zhang, J. He, *Macromolecules* **2005**, *38*, 8272.
[39] Q. Ren, J. Wu, J. Zhang, J. He, M. Guo, *Acta Polym. Sin.* **2003**, *1*, 448.
[40] F. Hermanutz, F. Gähr, E. Uerdingen, F. Meister, B. Kosan, *Macromol. Symp.* **2008**, *262*, 23.
[41] Y. Fukaya, A. Sugimoto, H. Ohno, *Biomacromolecules* **2006**, *7*, 3295.
[42] R. C. Remsing, R. P. Swatloski, R. D. Rogers, G. Moyna, *Chem. Commun.* **2006**, 1271.

[43] J. S. Moulthrop, R. P. Swatloski, G. Moyna, R. D. Rogers, *Chem. Commun.* **2005**, 1557.
[44] A. Pinkert, K. N. Marsh, S. Pang, *Ind. Eng. Chem. Res.* **2010**, *49*, 11121.
[45] M. Mazza, D.-A. Catana, C. Vaca-Garcia, C. Cecutti, *Cellulose* **2009**, *16*, 207.
[46] S. J. Sachnov, P. S. Schulz, P. Wasserscheid, *Chem. Commun.* **2011**, *47*, 11234.
[47] K. H. Lee, S. Zhang, T. P. Lodge, C. D. Frisbie, *J. Phys. Chem. B* **2011**, *115*, 3315.
[48] S. Dasgupta, G. Stoesser, N. Schweikert, R. Hahn, S. Dehm, R. Kruk, H. Hahn, *Adv. Funct. Mater.* **2012**, *22*, 4909.
[49] V. Lockett, M. Horne, R. Sedev, T. Rodopoulos, J. Ralston, *Phys. Chem. Chem. Phys* **2010**, *12*, 12499.
[50] V. Lockett, R. Sedev, J. Ralston, M. Horne, T. Rodopoulos, *J. Phys. Chem. C* **2008**, *112*, 7486.
[51] M. Ha, J. W. Seo, P. L. Prabhumirashi, W. Zhang, M. L. Geier, M. J. Renn, C. H. Kim, M. C. Hersam, C. D. Frisbie, *Nano Lett.* **2013**, *13*, 954.
[52] M. D. McCluskey, S. J. Jokela, *J. Appl. Phys.* **2009**, *106*, 071101.
[53] W. Xie, C. D. Frisbie, *J. Phys. Chem. C* **2011**, *115*, 14360.
[54] B. D. Paulsen, C. D. Frisbie, *J. Phys. Chem. C* **2012**, *116*, 3132.
[55] S. Thiemann, S. Sachnov, S. Porscha, P. Wasserscheid, J. Zaumseil, *J. Phys. Chem. C* **2012**, *116*, 13536.
[56] H. Yuan, H. Shimotani, J. Ye, S. Yoon, H. Aliah, A. Tsukazaki, M. Kawasaki, Y. Iwasa, *J. Am. Chem. Soc.* **2010**, *132*, 18402.
[57] B. Sun, H. Sirringhaus, *Nano Lett.* **2005**, *5*, 2408.
[58] S. Thiemann, M. Gruber, I. Lokteva, J. Hirschmann, M. Halik, J. Zaumseil, *ACS Appl. Mater. Interfaces* **2013**, *5*, 1656.
[59] M. Voigt, M. Klaumünzer, H. Thiem, W. Peukert, *J. Phys. Chem. C* **2010**, *114*, 6243.